Neuron, Vol. 28, 165–181, October, 2000, Copyright ©2000 by Cell Press

Mechanisms for Activation and Antagonism of an AMPA-Sensitive Glutamate Receptor: Crystal Structures of the GluR2 Ligand Binding Core

Neali Armstrong and Eric Gouaux*
Department of Biochemistry
and Molecular Biophysics
Columbia University
650 West 168th Street
New York, New York 10032

Summary

Crystal structures of the GluR2 ligand binding core (S1S2) have been determined in the apo state and in the presence of the antagonist DNQX, the partial agonist kainate, and the full agonists AMPA and glutamate. The domains of the S1S2 ligand binding core are expanded in the apo state and contract upon ligand binding with the extent of domain separation decreasing in the order of apo > DNQX > kainate > glutamate ≅ AMPA. These results suggest that agonist-induced domain closure gates the transmembrane channel and the extent of receptor activation depends upon the degree of domain closure. AMPA and glutamate also promote a 180° flip of a trans peptide bond in the ligand binding site. The crystal packing of the ligand binding cores suggests modes for subunit–subunit contact in the intact receptor and mechanisms by which allosteric effectors modulate receptor activity.

Introduction

The transduction of external signals across the cellular membrane and into the cytoplasm is a process fundamental to the evolution, development, and function of all living organisms. In the case of the mammalian nervous system, fast synaptic transmission between nerve cells is primarily carried out by ionotropic glutamate receptors (iGluRs), a class of transmembrane proteins that form glutamate-gated ion channels. In response to glutamate released by a presynaptic cell, the transmembrane gate of iGluRs briefly opens, depolarizing the postsynaptic cell and generating a receptor potential. A receptor potential of sufficient strength will trigger an action potential that will in turn propagate the initial stimulus. Even though iGluRs and other families of ligand-gated ion channels such as cyclic nucleotide-gated channels (Zagotta and Siegelbaum, 1996), nicotinic acetylcholine, γ-aminobutyric acid and glycine receptors (Unwin, 1998), and P2X receptors (North and Barnard, 1997) are fundamental components of many eukaryotic organisms, there is little understanding of the structural basis for agonist and antagonist action at these receptors.

iGluRs define a family of receptors for which there are three primary subgroups distinguished by amino acid sequence, pharmacological profile, functional behavior, and biological role (Seeburg, 1993; Hollmann and Heinemann, 1994; Nakanishi and Masu, 1994; Dingledine et al., 1999). Receptors that are most sensitive to the synthetic agonist α-amino-3-hydroxy-5-methyl-4-isoxazole propionic acid (AMPA) are so-called AMPA receptors (GluR1-4; Borges and Dingledine, 1998); receptors activated by the naturally occurring neurotoxin and agonist kainate have been deemed kainate receptors (GluR5-7, KA1-2; Lerma et al., 1997; Chittajallu et al., 1999); and receptors that require both glycine and glutamate for activation, but are also activated by synthetic *N*-methyl-D-aspartate, have been named NMDA receptors (NMDAR1, NMDAR2a–d; Yamakura and Shimoji, 1999). Although the "orphan" δ1 and δ2 receptors (Lomeli et al., 1993) neither bind glutamate nor form homomeric channels, they are nevertheless implicated in motor coordination (Kashiwabuchi et al., 1995), and mutations in these receptors can dramatically perturb central nervous system function (Zuo et al., 1997). Notwithstanding variations in sequence and function, the overarching similarities between AMPA, kainate, and NMDA receptors suggest that our studies of the mechanisms for agonist and antagonist action at AMPA receptors may be directly applicable to kainate and NMDA receptors and may be generally useful in the understanding of other classes of ligand-gated ion channels.

AMPA receptor agonists elicit a range of peak, steady-state, and single-channel currents and have widely varying equilibrium dissociation constants. On the one hand, AMPA and glutamate evoke similar electrophysiological responses even though AMPA binds ~20-fold more tightly than glutamate, depending on the receptor subtype (Andersen et al., 1996; Bräuner-Osborne et al., 2000). In whole-cell recordings saturating concentrations of AMPA and glutamate give rise to similar responses: they both produce large inward currents that rapidly desensitize to 1%–10% of the peak amplitude within tens of milliseconds, depending on the specific receptor (Kiskin et al., 1986; Trussell et al., 1988; Mosbacher et al., 1994; Partin et al., 1994; Koike et al., 2000). Single-channel studies also indicate that the amplitude of the conductance states elicited by AMPA and glutamate at recombinant AMPA receptors are similar (Swanson et al., 1997b). On the other hand, peak currents evoked by kainate acting at AMPA receptors are much smaller and rapidly desensitize to 70% of the peak amplitude (Patneau et al., 1993; Stern-Bach et al., 1998). Single-channel records from homomeric GluR4(i) receptors and heteromeric GluR2(i)/GluR4(i) receptors show that currents elicited by kainate are 4- to 8-fold smaller than those induced by glutamate or AMPA (Swanson et al., 1997b, but see also Smith et al., 2000). Thus, kainate is a partial agonist that produces rapid and limited desensitization at AMPA receptors (Kiskin et al., 1986; Patneau et al., 1993; Stern-Bach et al., 1998). At present there is no understanding, at the level of three-dimensional structure, of what distinguishes a partial agonist from a full agonist and a weakly bound agonist from a strongly bound agonist.

iGluRs are modular proteins composed of distinct ligand binding and channel-forming domains (Paas, 1998;

*To whom correspondence should be addressed (e-mail: jeg52@columbia.edu).

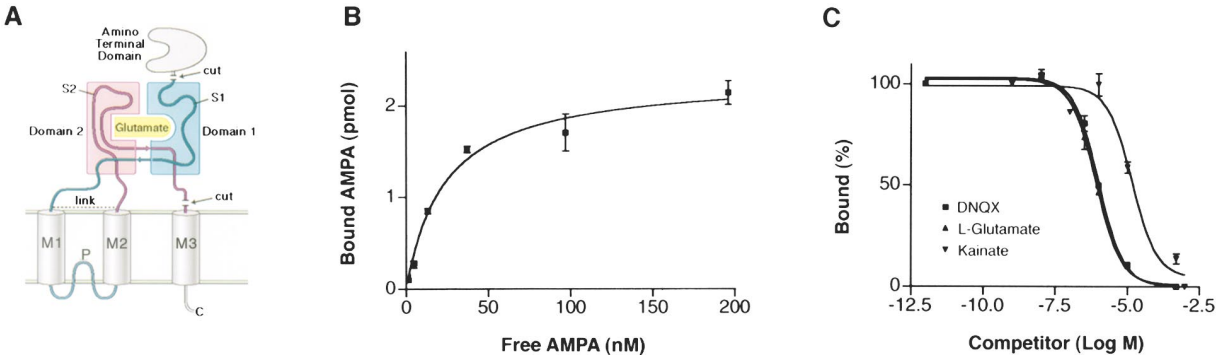

Figure 1. Ligand Binding Constants for S1S2J

(A) Domain structure of iGluRs showing the S1 and S2 segments in turquoise and pink, respectively. "Cut" and "link" denote the edges of the S1S2 construct.

(B) K_D for ^{3}H-AMPA binding was 24.8 ± 1.8 nM.

(C) IC_{50} for displacement of ^{3}H-AMPA by glutamate, kainate, and DNQX were 821 nM, 14.5 μM, and 998 nM, respectively.

Wo and Oswald, 1995). The agonist and antagonist binding site is localized to a clam shell–like ligand binding core (Kuusinen et al., 1995; Armstrong et al., 1998) that is connected to the three transmembrane segments (M1, M2, and M3) and reentrant loop (P) that form the ion channel. Eukaryotic iGluRs have an amino-terminal domain (ATD) that has low-level sequence identity to the bacterial leucine/isoleucine/valine binding protein (O'Hara et al., 1993). The ATD is not involved in ligand binding (Stern-Bach et al., 1994) but is important for subtype-specific assembly (Leuschner and Hoch, 1999) and mediates intersubunit interactions (Kuusinen et al., 1999). Between the end of the ATD and M1 is one half of the ligand binding core (S1), and located between M2 and M3 is the second half (S2). The S1S2 region, which has weak sequence homology to the bacterial periplasmic glutamine binding protein (QBP) (Nakanishi et al., 1990), contains the structural elements required to generate the wild-type responses to agonists and antagonists (Stern-Bach et al., 1994). In the cases of AMPA, kainate, and NMDA receptors, fusing S1 and S2 with a hydrophilic linker generates a water-soluble construct that retains wild-type ligand binding affinities (Kuusinen et al., 1995; Ivanovic et al., 1998; Keinänen et al., 1998). Development of large-scale refolding procedures for GluR2 S1S2 constructs produced as inclusion bodies in *Escherchia coli* (Chen and Gouaux, 1997) paved the way for the high-resolution crystallographic studies reported here.

The structure of GluR2 S1S2 complexed with kainate identified residues involved in kainate binding; located sites that modulate agonist specificity and affinity, as well as receptor desensitization; and mapped potential subunit–subunit contact sites (Armstrong et al., 1998). Nevertheless, the GluR2 S1S2-kainate structure left several important questions unanswered. How does the agonist-bound state differ from the apo or antagonist-bound state? Do full agonists produce greater domain closure than partial agonists? Do all structurally related agonists have identical modes of binding? How might agonist binding be linked to gating of the ionic channel? With these questions in mind, we developed a novel protein construct that enabled us to determine high resolution structures of GluR2 S1S2 in the apo state and in the presence of glutamate, AMPA, kainate, and the antagonist 6,7-dinitro-2,3-quinoxalinedione (DNQX).

Results

Construct Design and Structure Determination

To facilitate our crystallographic studies, we designed a novel construct of the GluR2 flop (Boulter et al., 1990; Sommer et al., 1990) ligand binding core (S1S2J) that contained a trypsin site 4 amino acids upstream of the first ordered residue in the S1S2I-kainate structure (Armstrong et al., 1998; Chen et al., 1998), a deletion of the last amino acid in S1 (Pro-507), and replacement of the 5 residue linker with the dipeptide Gly-Thr. Trypsinolysis of S1S2J yielded a 29.2 kDa fragment with the sequence GAN^{392}KT···, where the GluR2 sequence begins with Asn-392 and ends at Ser-775 (numbered according to the predicted mature GluR2 sequence; Keinänen et al., 1990). The K_D for ^{3}H-AMPA binding to S1S2J and the IC_{50} values for its displacement by glutamate, kainate, and DNQX indicate that S1S2J has ligand binding properties similar to those determined for longer GluR2 S1S2 constructs (Chen and Gouaux, 1997) and for the full-length receptor (Keinänen et al., 1990; Andersen et al., 1996; Hennegriff et al., 1997), as illustrated in Figure 1. Crystals of the S1S2J variant in complexes with a series of ligands diffract to high resolution, as summarized in Table 1.

The S1S2I-kainate structure (Armstrong et al., 1998) was the search probe in the molecular replacement (MR) solutions of the S1S2J-glutamate and -kainate structures. Although a promising molecular replacement solution for the DNQX complex was obtained using the S1S2I-kainate structure, the resulting model could not be refined below a R_{free} of 0.40. Therefore, the S1S2J-DNQX structure was solved by multiwavelength anomalous diffraction phasing (MAD; Hendrickson, 1991), using phases from the MR solution to determine the selenium positions of a selenomethionine derivative (Hendrickson et al., 1990). The S1S2J-DNQX structure, in turn, enabled the solution of the apo crystal form by MR. The electron density is continuous from Lys-393 to Cys-773 for all of the structures, and the density for the ligands and contacting residues is well resolved. Crystallographic

Table 1. Data Collection Statistics

Ligand	Spacegroup	Unit Cell (Å)	No. per a.u.[a]	Lambda (Å)	d_{min} (Å)[c]	Total Obs.	Unique Obs.	R_{merge}[b,d] (%)	Completeness[d] (%)
Glutamate	$P2_12_12$	$a = 114.0, b = 163.4, c = 47.4$	3	1.54	1.9 (1.97)	391030	69601	4.2 (19.9)	98.3 (87.8)
AMPA	$P2_12_12$	$a = 113.8, b = 163.2, c = 47.2$	3	0.979	1.7 (1.76)	503581	91073	6.8 (10.8)	93.5 (67.7)
Kainate (I)	$P2_1$	$a = 43.4, b = 63.1, c = 46.4, \beta = 92.3°$	1	0.918	1.6 (1.66)	154641	31151	3.0 (5.9)	94.4 (70.4)
Kainate (J)	$P2_12_12$	$a = 57.3, b = 89.0, c = 48.9$	1	1.54	1.9 (1.97)	96421	18725	3.3 (13.7)	92.0 (61.9)
Se-Met DNQX	$P2_12_12_1$	$a = 62.2, b = 92.6, c = 195.2$	4						
(e1-edge)				0.9795	2.5 (2.59)	138851	29669	5.9 (10.6)	74.4 (29.5)
(e2-peak)				0.9790	2.5 (2.59)	133161	29001	7.4 (10.9)	72.9 (28.9)
(e3-remote)				0.9687	2.5 (2.59)	158110	30771	7.4 (10.1)	77.4 (36.4)
DNQX	$P2_12_12_1$	$a = 62.2, b = 93.7, c = 97.4$	2	0.979	1.8 (1.86)	298773	50796	5.3 (8.4)	95.0 (83.8)
Apo	$P2_12_12_1$	$a = 62.2, b = 91.6, c = 98.4$	2	1.54	2.0 (2.07)	153854	37087	3.6 (14.8)	95.9 (73.7)

[a] Number of protein molecules per asymmetric unit (a.u.).
[b] $R_{merge} = (\Sigma|I_i - \langle I_i \rangle|)/\Sigma_i|I_i|$, where $\langle I_i \rangle$ is the mean I_i over all symmetry-equivalent reflections.
[c] Values in parentheses define the low resolution limits for the last shell of data.
[d] Values in parentheses are for the last shell of data.

refinement statistics for all of the complexes are shown in Table 2.

DNQX and Apo States Contain an Expanded Binding Cleft

The domains of the ligand binding core have separated in the DNQX and apo structures relative to the S1S2I-kainate structure (Armstrong et al., 1998), revealing an expanded binding cleft. The four protein molecules in the apo and DNQX asymmetric units all have moderately different conformations (ApoA, ApoB, DNQXA, DNQXB; Figure 2A), as defined by the degree of domain closure, or separation of domains 1 and 2; superposition of individual domains yields low root-mean-square deviation (rmsd) values (0.22 Å) indicating that the basis of the conformational variability is in the orientation of the domains. On average, the DNQX-bound structures are ~2.5° more closed than the apo structures with the maximal change in domain closure (6.0°) occurring between ApoA and DNQXB. All subsequent structural comparisons were performed using the ApoA protomer (most "open" conformation) as the reference structure.

DNQX binds near the "top" of the cleft, stacks directly under Tyr-450, and forms hydrogen bonds with 4 residues in domain 1 and 1 residue in domain 2 (Figure 2C). The two carbonyl groups mimic the α-carboxyl group common to agonists, forming hydrogen bonds to Arg-485 and the hydroxyl and backbone amide of Thr-480. A DNQX amide nitrogen makes a hydrogen bond to the backbone carbonyl of Pro-478. The quinoxalinedione ring lays ~3.6 Å directly below and parallel to the aromatic ring of Tyr-450, thus maximizing π–stacking interactions. Glu-705 adopts an extended conformation in DNQXB with the γ-carboxyl group directly under the quinoxalinedione rings, while in DNQXA the γ-carboxyl of Glu-705 is bent slightly away from DNQX. The 6-nitro group interacts with Tyr-732 and a protein-bound water molecule, and the 7-nitro moiety is within hydrogen binding distance (2.95 Å) of the hydroxyl of Thr-686.

There is strong omit map density (5σ) in the binding cleft at the base of helix F in both molecules in the asymmetric unit of the DNQX crystal form. A sulfate was modeled into this density in DNQXB based on its tetrahedral shape and intensity (Figure 2B). The sulfate interacts with helix F via 3 hydrogen bonds to the protein and 3 hydrogen bonds to solvent molecules, mimicking the interactions that the anionic "R" groups of agonists make with the base of helix F. Located between DNQX and the bound sulfate is a water molecule. The density in the binding site of the DNQXA polypeptide chain, although relatively strong, is elongated in shape, does not resemble a single sulfate ion, and has not been modeled. The DNQX and apo crystallization conditions contained ~0.25–0.4 M ammonium sulfate, but there is no evidence for a bound sulfate at the base of helix F in apo electron density maps.

In comparing the apo and the DNQX-bound structures, the major difference in the binding pocket residues involves Glu-705, which is the counter ion for the α-amino group of kainate (Armstrong et al., 1998). In the apo state, Glu-705 forms a salt bridge with Lys-730 and a hydrogen bond with Thr-655 (helix F). However, in the DNQXB structure, the carboxyl group of Glu-705 has rotated by ~135° about its Cβ-Cγ bond such that the

Table 2. Refinement Statistics

Complex	Resol. (Å)	R_{work}[a] (%)	R_{free}[b] (%)	No. Protein Atoms	No. Water	No. Lig Atoms	No. Ions	Average B-Value			Rms deviations		B-Values	
								Overall	Main	Ligand	Bonds (Å)	Angles (°)	Bonds	Angles
Glutamate	20–1.9	22.8	26.6	5894	265	30	5	20.26	19.15	13.72	0.011	1.517	2.4	3.4
AMPA	20–1.7	20.9	24.8	5872	420	39	5	17.13	15.41	13.35	0.010	1.454	2.1	3.1
Kainate (I)	20–1.6	21.6	26.1	1878	250	15	0	18.00	15.91	9.97	0.009	1.441	1.8	2.7
Kainate (J)	20–2.0	24.5	30.8	1885	88	15	0	30.90	30.93	28.50	0.011	1.697	2.5	3.6
DNQX	20–1.8	21.9	27.2	3851	363	36	5	14.74	13.07	26.08	0.010	1.421	2.1	3.0
Apo	20–2.0	22.4	28.7	3868	246	0	0	16.65	15.64	–	0.011	1.586	2.8	3.8

[a] $R_{work} = (\Sigma\ ||F_o| - |F_c||)/\Sigma|F_o|$, were F_o and F_c denote observed and calculated structure factors, respectively.
[b] Ten percent of the reflections in the DNQX, Apo, Kainate (J), and AMPA data sets and 5% of the reflections in the Glutamate and KainateJ data sets were set aside for the calculation of the R_{free} value.

carboxyl group is brought to the center of the binding cleft and away from Lys-730 and Thr-655 (Figure 2A). The orientation of Glu-705 in DNQXA is intermediate between the conformation of Glu-705 in the apo state and in DNQXB.

Modes of Agonist Binding: Glutamate, AMPA, and Kainate Structures

Glutamate, AMPA, and kainate, like most glutamate receptor agonists, are amino acids; the α-carboxyl and α-amino groups directly interact with the ligand binding core through 7 ion pair and hydrogen bonding interactions to domains 1 and 2 (Figure 3). While Arg-485 in domain 1 is the primary anchor for the α-carboxyl group, the backbone NH groups of Thr-480 (domain 1) and Ser-654 (domain 2) provide additional hydrogen bonds. Arg-485 is conserved in all glutamate receptors, and when mutated to a lysine in GluR1 (Kawamoto et al., 1997) or in GluR4-S1S2 (Lampinen et al., 1998), AMPA binding is abolished. The equivalent mutation in NR2B also destroys agonist-evoked currents in the NMDA receptor complex (Laube et al., 1997).

The α-amino group is secured to domains 1 and 2 by way of a nearly tetrahedral arrangement of interactions from the backbone carbonyl oxygen of Pro-478, the hydroxyl of Thr-480, and a carboxylate oxygen of Glu-705. Evidence for the importance of the ion pair interaction between the α-amino group and Glu-705 comes from an experiment which showed that ^{3}H-AMPA binding cannot be detected when this residue is mutated to glutamine in GluR4 S1S2 (Lampinen et al., 1998). Superpositions of the glutamate, AMPA, and kainate structures show that the fundamental interactions between the α-carboxyl and -amino groups and Arg-485, Glu-705, Thr-480, Ser-654, and Pro-478 are conserved between these three agonists (Figures 3B and 3C).

By contrast to the equivalent and well-defined receptor binding sites for the α-substituents of the agonists, the binding sites for the anionic moiety attached to the γ carbons of glutamate, kainate, and AMPA are surprisingly distinct. This distinction is not only because there are a number of solvent-mediated interactions but also because the positions of interacting waters and side chains vary in the complexes. In essence, the "γ" group binding pocket is composed of four subsites (D, E, F, and G in Figure 3D). Subsites D and E are located at the base of helix F and are formed by the backbone NH groups of Ser-654 and Thr-655, the hydroxyl of Thr-655, a water molecule bound to the base of helix F (water #3), and a water molecule (#2) tethered to the NH group of Leu-650 and the carbonyl oxygen of Leu-703. The γ-carboxyl groups of glutamate and kainate interact with the hydrogen bond donors in subsites D and E nearly identically (Figure 3B). The main difference between the glutamate and kainate binding clefts is the position of Leu-650, which moves substantially further into the cleft (3.0 Å) in the glutamate-bound state. Interestingly, the superposition in Figure 3B shows that the kainate isopropenyl group, which protrudes from the binding pocket, would sterically clash with Leu-650 in the glutamate-bound conformation.

Superposition of the AMPA and glutamate structures shows that the "γ" substituents are bound to the sub-

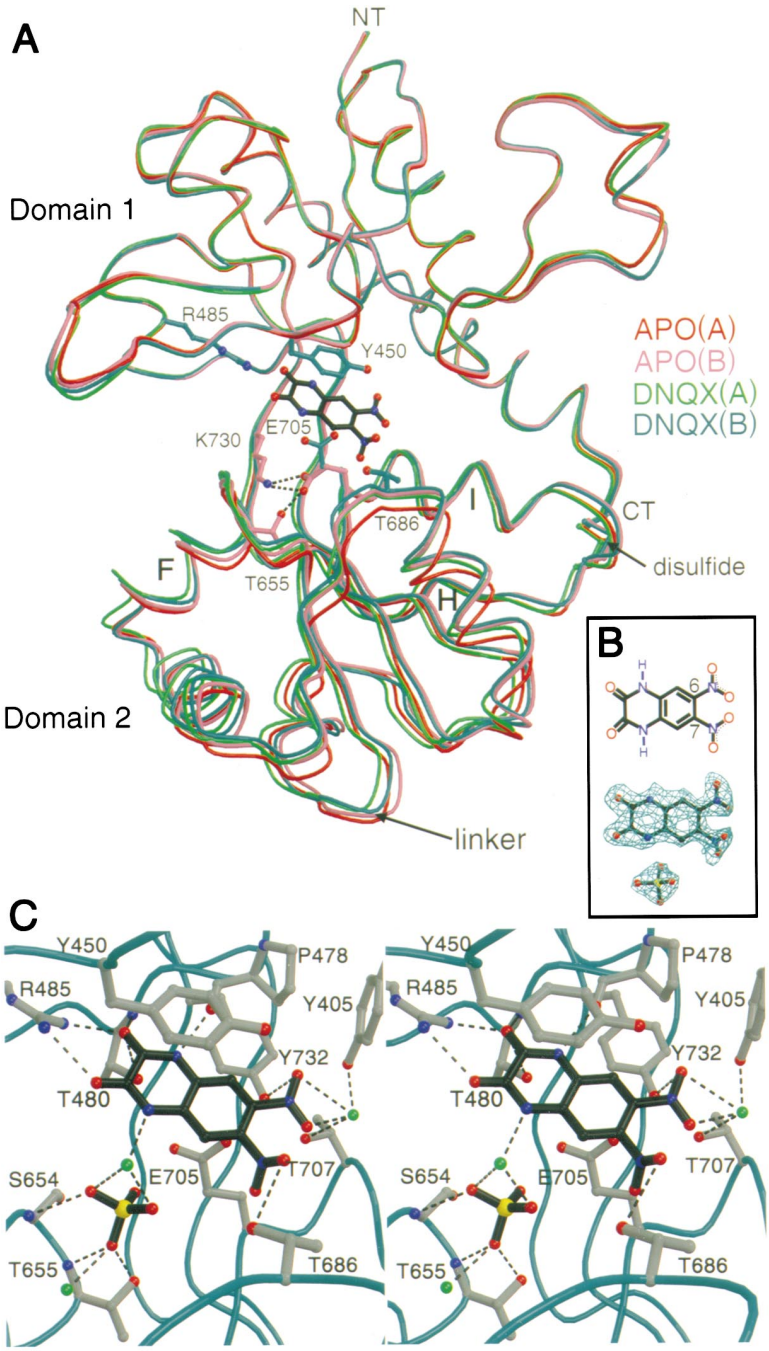

Figure 2. Superposition of the Expanded Cleft Structures and Stereo View of the DNQX Binding Site

(A) The two apo molecules (ApoA and ApoB) and two DNQX molecules (DNQXA and DNQXB) in each asymmetric unit were superimposed using only Cα atoms from domain 1. Apo protomers are shaded red and pink while DNQX protomers are colored light green and dark green. DNQX is depicted in black, and selected side chains from DNQXB are shown in dark green. The conformational change undergone by Glu-705 is illustrated by comparing its orientation in ApoB and DNQXB. In the apo state, Glu-705 accepts hydrogen bonds from the side chains of Lys-730 and Thr-655.

(B) The chemical structure of DNQX and F_o-F_c omit electron density for DNQX and sulfate contoured at 2.5 σ.

(C) Stereo image of the interactions between DNQX, sulfate, and S1S2J. DNQXB side chains are colored gray. Water molecules are shown as green balls. DNQX is colored black. Hydrogen bonds between DNQX, sulfate, and S1S2J are indicated by black dashed lines.

sites in different orientations (Figure 3C), in contrast to a prediction that the AMPA isoxazole moiety is bioisosteric to the glutamate γ-carboxyl group (Honoré and Lauridsen, 1980). Rather than occupying subsites D and E like the γ-carboxyl of kainate and glutamate, the isoxazole ring of AMPA binds in subsites E, F, and G. In the AMPA complex, subsite D is occupied by a water molecule (#4) that forms a close interaction with the isoxazole hydroxyl (2.45 Å), an α-carboxyl oxygen, and residues at the base of helix F. The recruitment of water #4 by AMPA thus transforms AMPA into a faithful bioisosteric mimic of glutamate. By also occupying subsite F, the isoxazole nitrogen displaces water #1 and makes a hydrogen bond to the backbone NH of Glu-705. The 5-methyl group of AMPA binds in subsite G, partially filling a hydrophobic pocket in domain 1 created by the reorientation of Met-708 and the side chain atoms of Pro-478 and Tyr-405. Met-708, which is in an extended conformation in the kainate and glutamate structures, undergoes a rotamer change in order to accommodate AMPA binding (Figure 3C).

Full Agonists Induce More Domain Closure Than Partial Agonists

The domains of the ligand binding core close upon agonist binding, sequestering the agonist in the cleft. Rela-

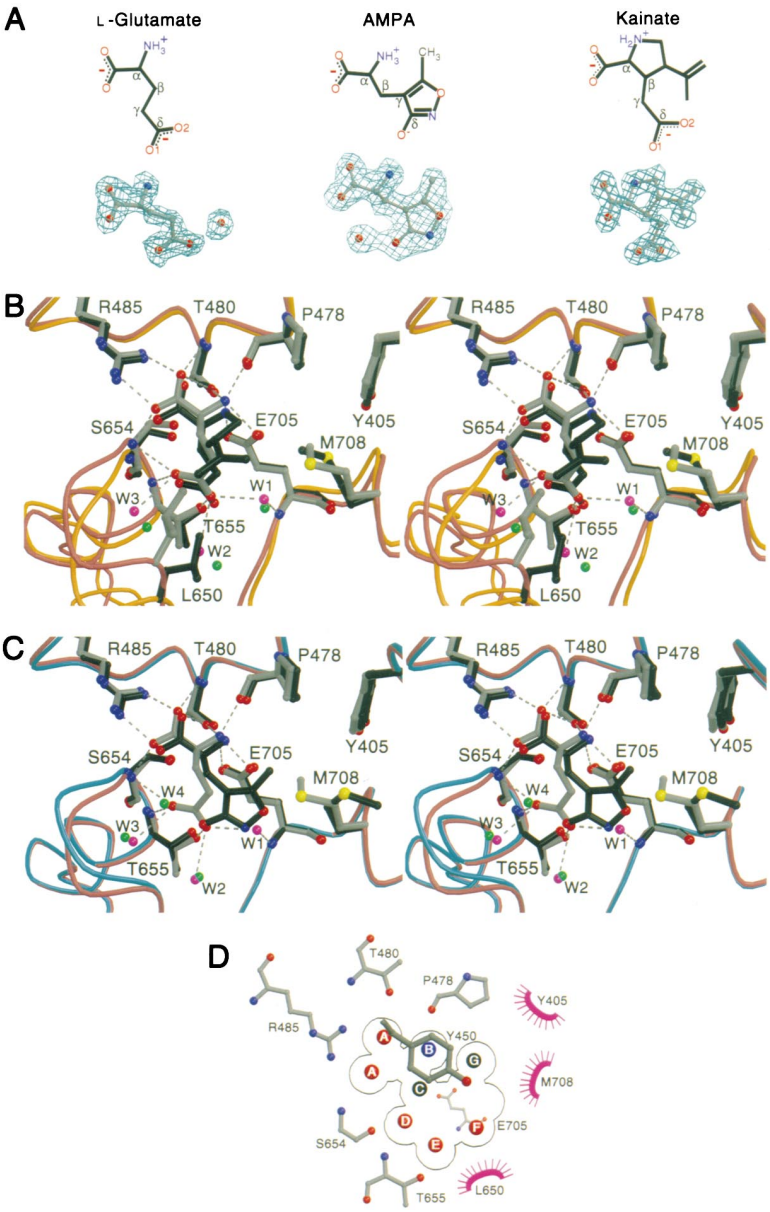

Figure 3. Modes of Agonist Binding

(A) F_o-F_c omit electron density and chemical structures for glutamate, AMPA and kainate in addition to selected water molecules. Maps are contoured at 3.0 σ.

(B) Stereo view of the binding cleft in superimposed glutamate and kainate structures. The glutamate backbone is colored pink, and the side chains and ligand are colored gray. The kainate backbone is shown in orange, while the side chains and ligand are black. The superposition was calculated using Cα atoms from domain 1. Only hydrogen bonds between glutamate and S1S2J are shown in (B) and (C). Selected water molecules in the glutamate and kainate structures are drawn in pink and green, respectively. Tyr-450 is omitted from (B) and (C) for clarity; the side chain is positioned directly over the binding site in this orientation (see [D]).

(C) Stereo view of the binding cleft in superimposed glutamate and AMPA structures. The glutamate structure is colored as in (B). The AMPA backbone is drawn in blue, and the side chain and ligand are colored black. The superposition was performed using all Cα atoms. Waters within hydrogen bonding distance of AMPA are shown as green balls.

(D) Schematic of the agonist binding site. For simplicity, all residues except Tyr-450 and Glu-705 have been flattened onto the plane of the page using the program LIGPLOT (Wallace et al., 1995). To represent the 3D nature of the binding cleft, Tyr-450 and Glu-705 are shown over and under the agonist subsites, respectively. Subsites drawn in red (A, D, E, and F) are occupied by hydrogen bond acceptors, while subsite B (blue) is occupied by a hydrogen bond donor.

tive to the ApoA conformation, AMPA and glutamate induce ~20° of domain closure while kainate induces only ~12° (Figure 4). In other words, the full agonists AMPA and glutamate bring domains 1 and 2 ~8° closer together than the partial agonist kainate. Unlike the moderate differences in domain closure observed in the apo and DNQX structures, the orientations of domains 1 and 2 in the six independent AMPA and glutamate complexes are similar. The two independent kainate structures are identical within experimental error and thus have a similar degree of domain closure. The substantial conformational change that occurs upon glutamate binding reduces the calculated radius of gyration by 0.8 Å relative to the apo state.

In general terms, the rotation describing the domain closure motion occurs about an axis that runs through the two interdomain β strands and along helix I, as illustrated in Figure 4. Significant changes (20°) in backbone torsion angles occur between Ser-497 and Ile-500 in the first strand and Leu-727 and Gly-731 in the second strand for both the apo to kainate and apo to AMPA/glutamate transitions. Smaller backbone torsion angle changes also occur at the C-terminal end of helix I between Arg-715 and Asp-719. As the location of the rotation axis suggests, helix I from domain 2 reorients with domain 1, while the remainder of domain 2 moves as a separate rigid body, perhaps because helix I is linked via a disulfide bond to domain 1. In the apo to kainate transition, the rotation axis runs between the two lobes and intersects the end of helix I, whereas in the apo to AMPA/glutamate transition, the rotation axis runs approximately down the center of helix I.

The Peptide Bond between Asp-651 and Ser-652 Adopts Multiple Conformations

Concomitant with the ~20° of domain closure induced by AMPA is a rearrangement of the protein backbone between Asp-651 and Gly-653 (Figure 5). In particular,

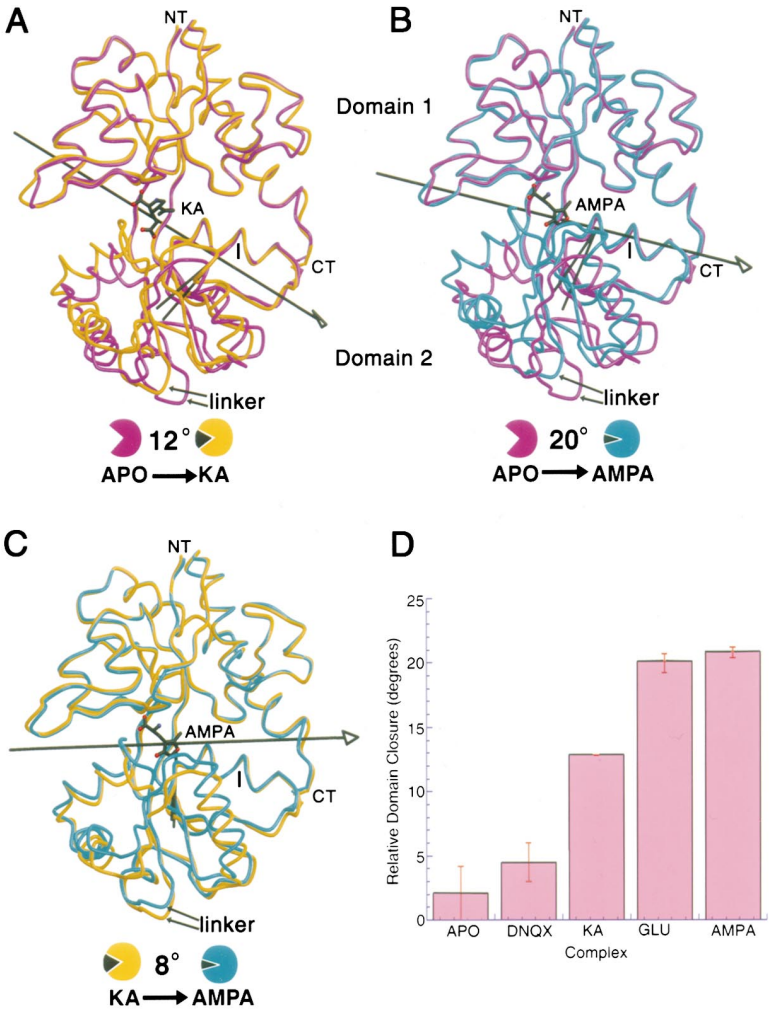

Figure 4. Relative Domain Closure and Corresponding Axes of Rotation for Important Structural Transitions

All of the superpositions were calculated using only Cα atoms from domain 1. The S1S2J backbones are colored according to the schematics at the bottom of the figure. The values listed below the superpositions are the relative extents of domain closure, in degrees.

(A) Superposition of apo and kainate (KA) structures.

(B) Superposition of apo and AMPA structures.

(C) Superposition of kainate and AMPA structures.

(D) Plot of the mean domain closure for the five complexes. All domain closure values were determined using ApoA as the reference (0°). The three molecules in the AMPA and glutamate a.u. and the two molecules in the DNQX and apo a.u. were used to determine the mean domain closure. For the kainate complex, the mean was calculated for the S1S2I and S1S2J structures. The error bars indicate the minimum and maximum domain closure values.

the *trans* peptide bond connecting Asp-651 and Ser-652 undergoes a ~180° flip relative to its orientation in the kainate, DNQX, and apo structures. Using the ApoA and the AMPA(A) protomers as a representative example, we find that the peptide bond flip occurs via a 180° change in ψ at Asp-651 and a 157° rotation in ϕ at Ser-652. In addition, ψ changes by 80° at Ser-652 and ϕ changes by 64° at Gly-653. Although neither Asp-651, Ser-652, nor Gly-653 directly interacts with ligands, these residues are flanked by Leu-650 and Ser-654, which form hydrophobic and hydrogen bonding interactions with agonists. The peptide bond rearrangement results in two additional hydrogen bonds between domains 1 and 2 in the AMPA-bound state; the backbone carbonyl of Ser-652 hydrogen bonds to the backbone amide of Gly-451, and a water-mediated hydrogen bond connects the backbone carbonyl of Asp-651 to the backbone amide of Tyr-450. All three molecules in the asymmetric unit of the AMPA crystal form clearly contain the flipped peptide orientation. Glutamate also is capable of inducing the peptide bond flip, albeit less effectively than AMPA. In the glutamate cocrystals, protomer A is in the unflipped conformation and protomer C is in the flipped conformation. The electron density for this region in protomer B is not well defined, probably because multiple conformations are occupied.

A 2-Fold Symmetric Dimer Is Formed by Crystal Packing Interactions

In all five of the crystal forms obtained using the S1S2J construct, the protein molecules pack in such a manner as to produce a 2-fold symmetric "dimer." As shown in Figure 6A, the two protomers are oriented with both N termini along the upper face of the dimer, both linker regions are on the bottom face, and both binding sites are facing outward. Domain 1 from each of the 2-fold related protomers comprises the dimer interface, which has both hydrophobic and polar interactions and is made up of helices D and J and the first interdomain β strand. The interface is similar between all five structures; for example, superposition of the apo and the AMPA noncrystallographic symmetry (NCS)-dimers using α-carbons from domain 1 of each protomer yields an rmsd of 0.68 Å.

The "dimer" interface buries 1150 Å^2 of solvent-accessible surface area per protomer and contains 2 salt bridges and 8 hydrogen bonds. Leu-483, which blocks desensitization when mutated to Tyr in GluR3 (Stern-Bach et al., 1998), forms a hydrophobic cluster with the conserved residues Leu-748 and Leu-751 on helix J of the adjacent protomer (Figure 6C); Leu-483 also makes a number of van der Waals contacts $<$ 3.8 Å with Lys-752, which is located on helix J of the 2-fold related

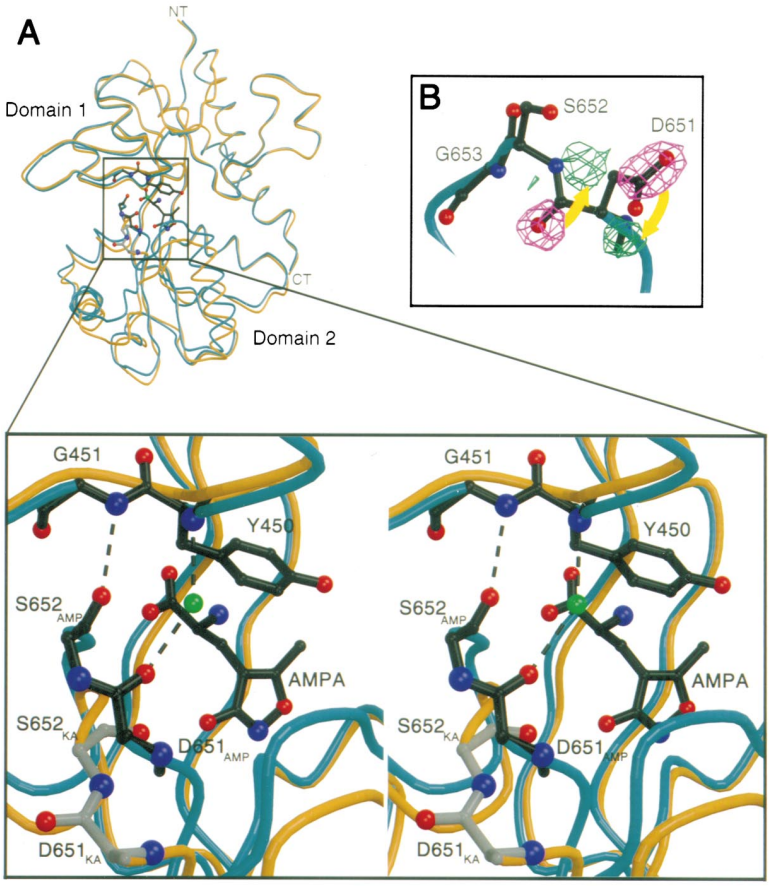

Figure 5. The Peptide Bond Flip in the AMPA Structure

(A) The superposition of the kainate and AMPA structures is exactly as in Figure 4C. The stereo diagram illustrates residues involved in peptide bond flipping. Side chains from the kainate and AMPA structures are drawn in gray and black, respectively. The side chains for Asp-651 and Ser-652 have been omitted for clarity. A water molecule in the AMPA structure that mediates a hydrogen bond between the carbonyl of Asp-651 and the amide of Tyr-450 is drawn as a green ball. (B) Positive (green) and negative (pink) density from an F_o-F_c electron density calculated using F_c coefficients from an "unflipped" AMPA model. The yellow arrows illustrate the movement of the Asp-651 carbonyl and side chain carboxylate to their appropriate positions. The "unflipped" model is drawn with the electron density as opposed to the flipped orientation depicted in (A).

molecule. A symmetric pair of salt links are formed between Glu-486, which is located in helix D of one protomer, and Lys-493, which is situated in the first interdomain β strand on the other protomer; Glu-486 and Lys-493 are conserved across all non-NMDA iGluRs. Glu-486 also accepts a hydrogen bond from the side chain of Asn-747, and Lys-493 donates a hydrogen to the backbone carbonyl of Phe-491. Asn-754, which is at a site that mediates cyclothiazide sensitivity in AMPA receptors (Partin et al., 1996), is partially buried in the dimer interface and forms an intermolecular hydrogen bond with the backbone carbonyl of Ser-729 on the 2-fold related protomer.

Histidine Side Chains Chelate Zinc in the Glutamate and AMPA Structures

The glutamate and AMPA complexes were crystallized in the presence of zinc acetate. Evidence from anomalous difference Fourier maps, which revealed the presence of five strong peaks of electron density (9–20 σ), together with the chemical environment of these density peaks, suggested that they were zinc ions. Four of the five zinc ions are located at interprotomer lattice contacts, while the fifth zinc is chelated by intraprotomer interactions between Glu-431 and His-435 of protomer C (Figure 6B). All six histidines in the asymmetric unit (two per protomer) contact a zinc ion. His-412 in loop 1 of protomers C and B* (asterisk indicates a symmetry-related molecule) in conjunction with Glu-419 (B*) coordinate one zinc; His-412 (A) and Asp-454 (C*) bind a second zinc; the third and fourth interpromoter sites are formed by His-435 (A), Glu-431 (A), and Glu-678 (B) and His-435 (B*), Glu-431 (B*), and Glu-678 (A).

Discussion

The structure-based design of a novel GluR2 S1S2 construct has redefined the S1 and S2 boundaries required to retain ligand binding activity and has facilitated the crystallization of the ligand binding core in the apo state and in the presence of DNQX, kainate, glutamate, and AMPA. These five structures provide the first views of the ligand binding core of a ligand-gated ion channel in conformations that may be associated with functional states of the channel, thus lending insight into receptor activation, antagonism, and the molecular basis for ligand specificity.

The Closed Channel State Contains an Expanded Binding Cleft

In the absence of ligand (apo) or in the presence of an antagonist, the gate of the transmembrane ion channel is closed. This resting state of the receptor, we suggest, possesses a ligand binding core in which domains 1 and 2 are separated and the receptor cleft is open, as seen in the apo and DNQX-complex structures reported here. In the apo state, the open-cleft conformation is stabilized by intradomain interactions, while the agonist

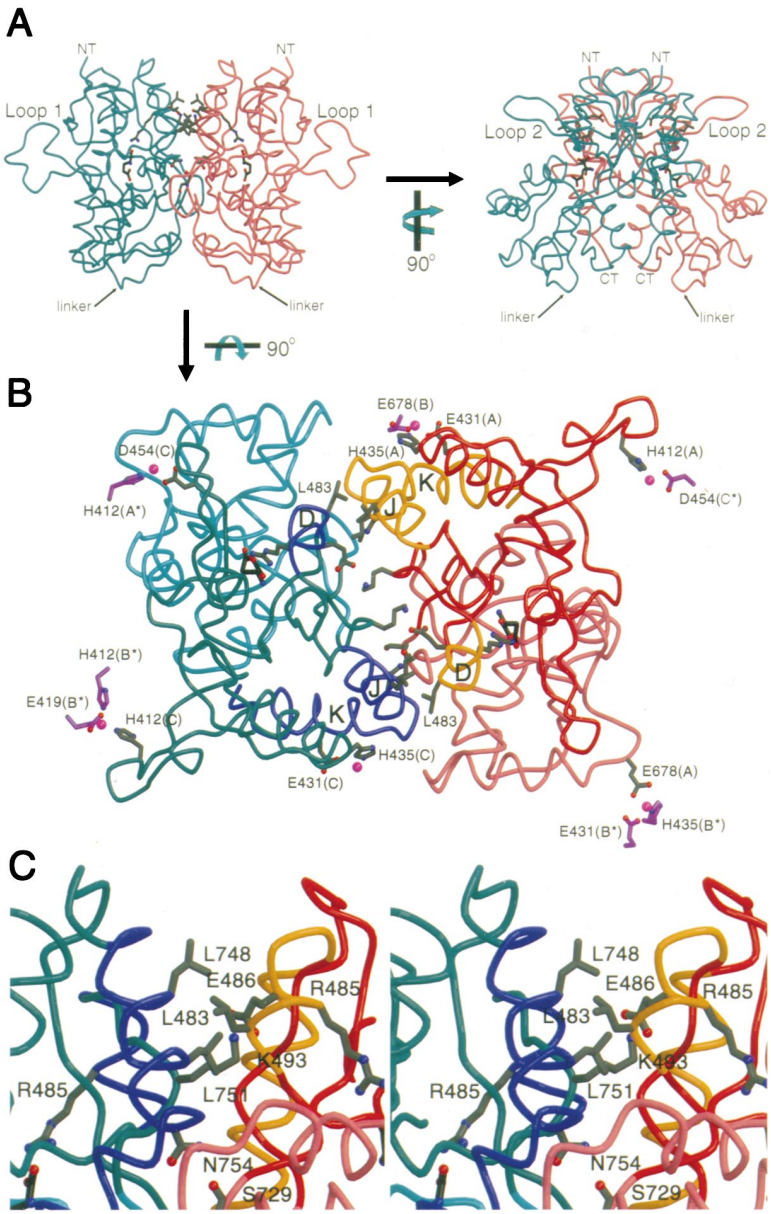

Figure 6. Crystal Packing Produces a S1S2J Dimer with 2-Fold Symmetry

(A) Side views of the noncrystallographic dimer formed by protomers A (pink) and C (green) in the glutamate structure. In these orientations, the 2-fold rotation axis runs vertically in the plane of the page. Residues making interprotomer contacts are colored gray. Note the proximity of Arg-485, which interacts with glutamate, to interface residues.

(B) Top view of the dimer looking down the 2-fold symmetry axis. Protomer C is on the left with domain 1 colored green, domain 2 colored cyan, and helices D, J, and K colored blue. Domain 1 in protomer A is shaded red, domain 2 is pink, and helices D, J, and K are in orange. Zinc ions are depicted by pink spheres. The residues that chelate the zinc ions in the dimer are gray. Symmetry-related residues (indicated by asterisk) that participate in zinc chelation are purple.

(C) Stereo diagram of the interactions between the protomers. The orientation is the same as in the left panel of (A). Similar interactions also occur in the dimer found in the S1S2J-apo, DNQX, kainate, and AMPA structures.

bound state(s) is stabilized by agonist-receptor and interdomain interactions. Glu-705, which is the counterion of the agonist α-amino group, is bound to Lys-730 and Thr-655, thus occupying the anion binding site at the base of helix F and disfavoring domain closure in the absence of ligand binding. Although related bacterial periplasmic ligand binding proteins, such as glucose/galactose binding protein and the histidine binding protein adopt closed-cleft conformations in the apo state (Flocco and Mowbray, 1994; Wolf et al., 1994), we suspect that the ligand binding cores of iGluRs do not behave in a similar manner due to intradomain interactions as described above and to intersubunit interactions in the intact receptor.

Competitive quinoxalinedione antagonists like DNQX "work" by occupying the sites to which the α-carboxyl and α-amino groups of agonists bind and, in comparison with AMPA, by overlapping with nearly all of the isoxazole ring binding site as well. By occupying the ligand binding cleft near the axis of rotation that describes the relative movement of domains 1 and 2 in the apo to AMPA transition, DNQX stabilizes the open-cleft conformation via antagonist–receptor interactions. The 7-nitro group of DNQX "braces" the clamshell-like S1S2 core in an open conformation by binding to Thr-686, thus completely blocking the interaction that Thr-686 on domain 2 would make with Glu-402 on domain 1 in an agonist-bound state (Armstrong et al., 1998). The larger quinoxalinedione antagonist 2,3-dihydroxy-6-nitro-7-sulphamoylbenzoquinoxaline (NBQX) probably binds more tightly because the 7-sulphamoylbenzo entity can interact with residues near Thr-686 in domain 2 (Honoré et al., 1988).

By contrast to the quinoxalinedione compounds, we suggest that amino acid–derived antagonists "brace" domains 1 and 2 in an open-cleft conformation by ex-

tending the length of the linker between the α-carbon substituents and the anionic "R" moiety, relative to agonists. For example, 2-amino-3-[5-tert-butyl-3-(phosphonomethoxy)-4-isoxazolyl]-propionic acid (ATPO) contains a ζ-phosphate (Moller et al., 1999) that probably interacts with the base of helix F, much like the sulfate anion in the GluR2 S1S2-DNQX complex. ATPO was readily modeled into the DNQX binding site by using the positions of the α-carbon substituents of AMPA in the AMPA cocrystals and the sulfate ion in the DNQX complex as guides. Indeed, there are a number of NMDA receptor antagonists that have the equivalent of 3–5 methylene groups between the α-carbon and the anionic "R" substituent (Wheal and Thomson, 1995), in comparison to the 2 methylene groups between the α-carbon and the γ-carboxyl group in glutamate.

Even though DNQX stabilizes the GluR2 ligand binding core in an open conformation, relative to the apo state DNQX does induce a modest extent of domain closure and promotes the local conformational rearrangement of Glu-705 to its agonist-state conformation. In the case of the wild-type receptor, these conformational changes do not result in channel activation. However, introduction of the so-called Lurcher mutation (Zuo et al., 1997) into GluR1 results in a receptor that is activated by CNQX, a compound closely related to DNQX and an antagonist of wild-type AMPA receptors (Taverna et al., 2000). This relatively subtle mutation of a single alanine to a threonine maps to a region of glutamate receptors and potassium channels that is near the predicted ion channel gate and not in the S1S2 constructs described here (Doyle et al., 1998; Chen et al., 1999; Perozo et al., 1999). We suggest that the Lurcher mutation results in a GluR1 receptor that is activated by a much smaller extent of domain closure, relative to the wild-type receptor. Different antagonists which have widely variable structures may yield varying degrees of domain closure and may thus elicit a range of agonist or antagonist activities at iGluRs containing Lurcher or Lurcher-like mutations (Kohda et al., 2000).

Channel Activation and Desensitization

On the basis of the structures reported here, we propose that substantial closure of the ligand binding cleft leads to activation (opening) of the ionic channel gate. Full agonists, such as glutamate and AMPA, maximally activate AMPA receptors, measured either in terms of peak current or in terms of steady-state currents in the presence of the desensitization blocker cyclothiazide, and they induce the same maximal extent of domain closure (see Figure 4). Kainate, in contrast to glutamate and AMPA, is a partial agonist at AMPA receptors, as determined from macroscopic (Patneau et al., 1993; Stern-Bach et al., 1998; Koike et al., 2000) and single-channel recordings (Swanson et al., 1997b). On the basis of the crystal structures of the two GluR2 S1S2 complexes with kainate, the 12° of domain closure seen in the kainate structures is substantially less (8°; see Figure 4C) than that produced by glutamate and AMPA (20°), suggesting a positive correlation between domain closure and receptor activation. Perhaps the intermediate domain closure elicited by kainate is translated into an intermediate conformation of the receptor at the transmembrane gate.

In contrast to a previous model for receptor activation (Mano et al., 1996), we propose that the activated state involves the interaction of agonists with both lobes of S1S2 and that the activated conformation is similar to our agonist-bound structures. If agonist binding to domain 1 were sufficient to activate the receptor, one might predict that kainate would activate AMPA receptors as fully as glutamate, since the contacts that kainate makes with domain 1 are very similar to those that glutamate makes. However, the interactions between kainate and domain 2 are what primarily distinguish kainate from glutamate and AMPA. Specifically, Leu-650 in domain 2 is in van der Waals contact with the isopropenyl group of kainate, thus preventing domain 2 from moving to a glutamate-like position (Figure 3B).

Activation of AMPA receptors is coupled to rapid desensitization, and receptor desensitization is accompanied by a ~5- to 10-fold increase in AMPA or glutamate affinity as determined by the effects of allosteric modulators on ligand binding (Kessler et al., 1996) and by analysis of nondesensitizing mutants (Stern-Bach et al., 1998). Indeed, the agonist affinities measured for the S1S2J construct studied here are most similar to the high-affinity binding state reported for presumably desensitized recombinant AMPA receptors. Thus, the conformations of the ligand binding core in the agonist-bound structures reported here may also be similar to the receptor's conformation in the equilibrium-desensitized state. However, based on the magnitude of estimated affinity differences between the nondesensitized and desensitized states, the energetic difference between the activated and desensitized states is small and on the order of 1–2 hydrogen bonds. Alternatively, small differences (1°–3°) in domain closure could also result in an overall modulation of agonist affinity. Because most of the residues that have been implicated in desensitization map to the S1S2 surface, it is likely that differences between the activated and desensitized states primarily involve intersubunit contacts that in turn result in small, but still significant, conformational changes in the ligand binding core. The difference in extent of desensitization observed for glutamate versus kainate (Patneau et al., 1993) is likely the result of differences in domain closure that in turn lead to differences in intersubunit contacts. Of course, studies that probe the structure of the intact receptor will ultimately be required to provide a definitive answer to the questions of domain closure and channel activation and desensitization.

Kainate receptors, which are fully activated by kainate, have a valine instead of a leucine at the position equivalent to 650 in GluR2. When the corresponding leucine is changed to a valine or a threonine in GluR1, the resulting mutants have EC_{50} values for kainate that are lower by 6- and 20-fold, respectively (Mano et al., 1996). The Leu to Thr mutant exhibited a ~2-fold greater potentiation by cyclothiazide in comparison to the wild-type receptor, suggesting that the mutation increased the extent of desensitization. Thus, in terms of desensitization, kainate acting on the mutant receptor has become more similar to the action of glutamate on wild-type receptors. Unfortunately, it is not clear how the mutation affects activation because the studies were not carried out with sufficient time resolution so as to accurately measure the peak currents. Modeling studies

(data not shown) show that replacing Leu-650 by valine or threonine allows the ligand binding core to adopt a glutamate-like conformation in the presence of bound kainate. The significantly lower EC_{50} for the threonine mutant is perhaps due to a hydrogen bond between the threonine hydroxyl and the γ-carboxyl of kainate. Therefore, we suggest that differences in the ligand binding pocket enable kainate to induce a similar degree of domain closure at kainate receptors as AMPA and glutamate induce at AMPA receptors, reinforcing the notion that activation is a conserved process across the iGluR family (Stern-Bach et al., 1998).

The substantial difference in conformation we see between the apo and agonist-bound structures stands in contrast to results obtained from small-angle x-ray scattering (SAXS) experiments on a longer GluR4 S1S2 construct that found no change in the radius of gyration in the presence and absence of agonist (Abele et al., 1999). Similar studies performed on the leucine/isoleucine/valine binding protein found a 1.0 Å decrease in R_g upon ligand binding (Olah et al., 1993) and for the related glutamine binding protein the calculated ΔR_g between the apo and liganded state is 1.3 Å (Hsiao et al., 1996; Sun et al., 1998). The reason for the discrepancy between the crystallography and SAXS experiments is unclear but may be due to differences in the S1S2 constructs or to heterogeneity in the conformation of the apo state. Stabilizing the open-cleft conformation by the addition of an antagonist may help to clarify results from SAXS experiments.

The GluR2 Ligand Binding Core Has Zinc Binding Sites

Vesicular zinc is particularly abundant in the hippocampus and cerebral cortex and is released, along with glutamate, during electrical stimulation (Perez-Clausell and Danscher, 1985). At selected hippocampal synapses, concentrations as high as 300 μM have been measured (Assaf and Chung, 1984). Micromolar concentrations of zinc potentiate currents from both native (Mayer and Vyklicky, 1989) and recombinant AMPA receptors (Dreixler and Leonard, 1994). Dreixler et al. (1994) found that in the presence of calcium, zinc enhanced kainate-induced currents on GluR3 but not GluR1 receptors (Dreixler and Leonard, 1994). In the AMPA and glutamate cocrystal structures described here, we find a number of zinc binding sites formed in part by histidine residues. Interestingly, His-412 is conserved in GluR2-4, whereas GluR1 contains an alanine at this position; His-435 is conserved throughout the AMPA receptor subunits. Although the mechanism(s) underlying the effects of zinc on AMPA receptors are unknown, our crystallographic data suggest that the histidine residues in S1S2 are candidates for zinc binding sites in the intact receptor that may, for example, bridge neighboring subunits and modulate receptor activity.

The Flipped Peptide Bond May Stabilize a Closed Binding Cleft

Numerous hydrogen bonding interactions between domain 1 and domain 2 are important for conferring affinity and specificity to agonist binding (Dingledine et al., 1999). When the Asp-651 and Ser-652 peptide bond flips from its conformation in the apo, DNQX, and kainate complexes to its conformation in the AMPA and glutamate complexes, two additional hydrogen bonds are formed between domains 1 and 2. These interactions knit the "roof" of the ligand binding site closed and may further stabilize the closed-cleft conformation. Interestingly, the AMPA and glutamate crystal forms, which are isomorphous and have similar lattice contacts, are not identical in terms of the conformation at the Asp-651 and Ser-652 peptide bond. AMPA may more effectively stabilize the flipped conformation because it binds more tightly and promotes slightly greater domain closure.

The precise role, if any, that the conformational variability at the Asp-651 and Ser-652 peptide bond plays in the activation, desensitization, or deactivation of the receptor is unclear. However, elements that stabilize the conformation of the agonist-bound receptor are likely to slow the rate of agonist release and deactivation. In the GluR2 S1S2 structure, adjacent to the Asp-651 and Ser-652 peptide bond is a site in kainate receptors (Asn-721 in GluR6) that is homologous to Thr-686 in GluR2 and mediates differences in domoate deactivation rates between GluR5 and GluR6 (Swanson et al., 1997a). By analogy to the kainate receptors, the interdomain hydrogen bonds that residues Asp-651 and Ser-652 make to domain 1 may also modulate receptor deactivation and agonist release. Although $\sim$180° rotations of *trans* peptide bonds are not common, there are a number of previously documented occurrences in which peptide bonds flip depending on the functional state of the protein (Nar et al., 1991; Romero et al., 1996; Emsley et al., 2000). In the case of iGluRs, our finding of the peptide bond flip at Asp-651–Ser-652 is novel, and it may provide yet another mechanism by which the activities of iGluRs are modulated.

The GluR2 Ligand Binding Core Forms a "Dimer" in the Crystal

The presence of a similar "dimer" in all six of the S1S2J crystal forms reported here is striking. Although the isolated ligand binding core is predominately monomeric in solution, as judged by size-exclusion chromatography and analytical ultracentrifugation (unpublished data), data from other groups on related receptors suggests that the extracellular domains of iGluRs may assemble in dimeric units. For example, Kuusinen et al. found that the entire extracellular domain of GluR4 behaves as a dimer on a size-exclusion column and in sucrose density gradients (Kuusinen et al., 1999). A NMDA receptor ligand binding core appears to adopt several oligomerization states, one of which is dimeric (Ivanovic et al., 1998). The ligand binding domain from the metabotropic glutamate receptors, which is homologous to the iGluR ATD, forms disulfide-linked dimers (Romano et al., 1996; Okamoto et al., 1998). Thus, the molecular symmetry of the extracellular portions of iGluRs may differ from the symmetry of the ion channel, the latter of which is probably 4-fold symmetric.

Determination of biologically relevant protein interfaces by analysis of crystal packing interactions is fraught with uncertainty, and the "dimer" we observe in our crystals may not be related to interfaces in the intact

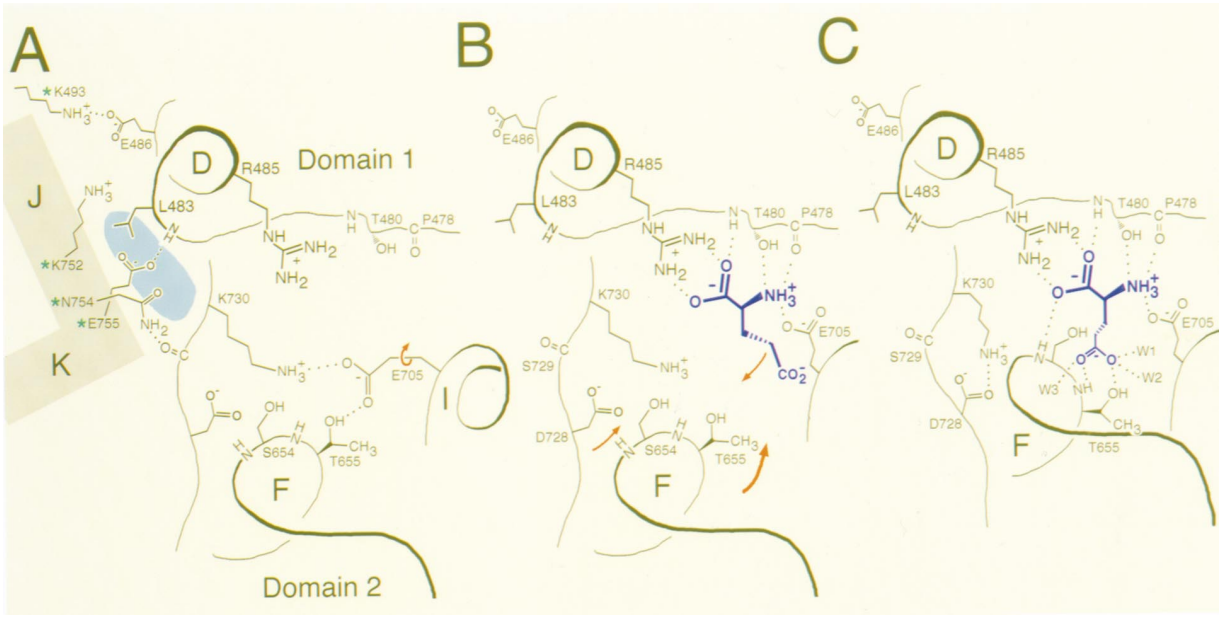

Figure 7. Mechanism of Glutamate Binding

Shown are the ligand binding sites in the apo (A), DNQX complex (B), and glutamate complex (C) states. Residues on a 2-fold related subunit are indicated by asterisks, and a solvent-filled cavity that might represent the binding site for cyclothiazide is depicted by a light blue ellipse and is located at the dimer interface. In (B) DNQX has been removed and glutamate has been modeled in its place in an effort to model a complex between the receptor and glutamate prior to domain closure.

receptor. By the standard criteria of buried surface area and the number of polar and nonpolar interactions (Conte et al., 1999), the S1S2J dimer interface is large with relatively few hydrogen bonds, an observation that may explain why dimers do not predominate in solution. Only further experiments will validate or refute the relationship between the S1S2J "dimer" observed in the crystals and the S1S2 interface(s) in the intact receptor.

Nevertheless, it has not escaped our attention that a number of residues implicated in receptor desensitization are clustered in the dimer interface. Leu-483 is located at a position that modulates receptor desensitization in GluR3; when the equivalent leucine in GluR3 is changed to tyrosine, the resulting mutant does not desensitize (Stern-Bach et al., 1998). In fact, introduction of any aromatic amino acid dramatically slows desensitization (Stern-Bach et al., 1998). Recent experiments have shown that mutation of Leu-483 in GluR2 to Tyr also produces a nondesensitizing receptor (M. Mayer, personal communication). In the dimer interface, the side chain of Leu-483 is in van der Waals contact with Lys-752. If we assume that the dimer interface we see in the crystal is relevant to the intact receptor, then the introduction of aromatic residues at position 483 might result in favorable cation–π interactions with Lys-752 on the 2-fold related subunit. A stabilizing interaction between residues at positions 483 and 752 may in turn slow desensitization.

Other sites in the dimer interface that also modulate receptor desensitization are Asn-754 and Gly-743. Asn-754 is a site that mediates allosteric regulation of desensitization in AMPA receptors by cyclothiazide (Partin et al., 1995); a simple Asn to Ser change is sufficient to confer sensitivity to cyclothiazide in the GluR1-flop isoform (Partin et al., 1996). In our structures, the amide side chain of Asn-754 makes an intersubunit hydrogen bond to the backbone carbonyl of Ser-729, a residue that is located near the interdomain hinge. Located on "top" of the dimer is a large depression that is near the arginine/glycine (R/G) RNA editing site that modulates the rate of receptor desensitization (Lomeli et al., 1994). The S1S2 constructs reported here have a glycine at this position; modeling arginines into the Gly-743 sites partially fills this hole and generates a positive electrostatic potential at the surface without creating any serious steric clashes. The dimer interface observed in our crystals illustrates how sites implicated in receptor desensitization are juxtaposed across from the ligand binding cleft of an adjacent subunit; perhaps one mechanism underlying receptor desensitization involves the modulation of interactions between helices J and K of one subunit and the ligand binding cleft of another subunit.

A Subsite Map of the Agonist Binding Cleft

On the basis of conserved locations of the agonist hydrogen bond donors and acceptors as well as hydrophobic groups, we have defined seven positions (Figure 3D) within the binding cleft that are common interaction sites for AMPA receptor agonists. We predict that the α-carboxyl and α-amino groups of all AMPA receptor agonists will occupy sites A and B, respectively. The region of the agonist linking the zwitterion to the γ-anionic moiety is positioned in site C and will form hydrophobic interactions with Tyr-450. Sites D and E are occupied by the γ-carboxyl oxygens from glutamate and kainate. These sites connect the agonist to Ser-654 and Thr-655 in domain 2. The sixth site (F) is occupied by a moiety

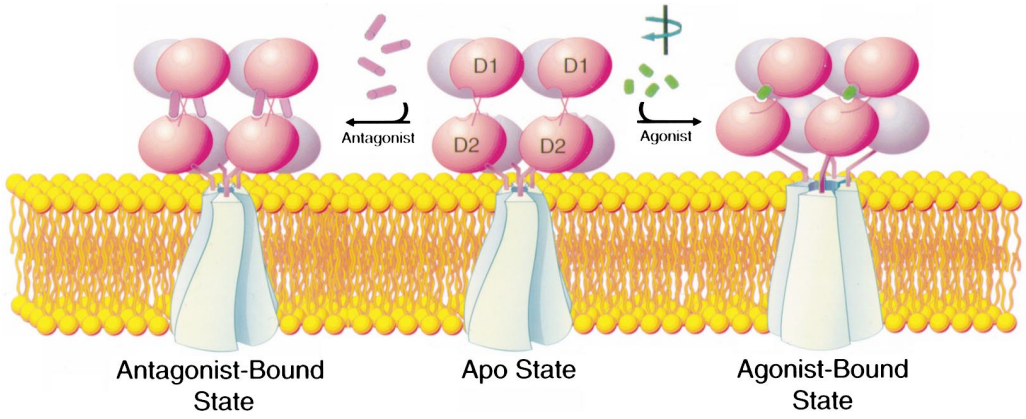

Figure 8. A Model for Glutamate Receptor Activation and Antagonism

The tetramer model was constructed by placing two dimers side by side (orientation as in the right side of Figure 6A), so that the interdimer 2-fold is in the center of the 4 subunits and coincides with the channel 4-fold. The dimensions of this dimer-of-dimers arrangement is ~80 Å × 55 Å × 50 Å (l × w × h). Each dimer is composed of a pink and a purple S1S2 core. Domain 1 and domain 2 are labeled as D1 and D2, respectively. The channel region depicted here encompasses M1–3 and the P region. The ATD has not been modeled.

(water in the glutamate and kainate complexes, isoxazole nitrogen in the AMPA structure) that will link the agonist to the backbone amide of Glu-705. Site G is the hydrophobic pocket in domain 1. From our structures, only the 5-methyl substituent from AMPA occupies this site. However, if a few side chains undergo modest rearrangements, the pocket could accommodate the t-butyl group from ATPA (Matzen et al., 1997). Thus, agonist atoms in sites A and B form polar interactions with domain 1, while subsites D, E, and F form hydrogen bonds with domain 2. We anticipate that subsites A–F will always be occupied with either agonist atoms or water molecules, while only some agonists will fill site G. Only the isopropenyl group from kainate does not occupy any of these subsites; perhaps agonists with substituents outside this subsite map will be partial AMPA receptor agonists.

Mechanism of Ligand Binding and Coupling to Channel Gating

The series of structures presented here allow us to develop a mechanism for glutamate binding to the ligand binding core, as illustrated in Figure 7. In the apo state, the ligand binding cleft is open, domains 1 and 2 are separated, and Glu-705 is bound to the base of helix F and to Lys-730. Using the DNQX structure as a model for the initial receptor-glutamate complex, we suggest that glutamate binds to domain 1 via interactions between its α-amino and α-carboxyl groups and Arg-485, Thr-480, Pro-478, and Glu-705, in agreement with previous studies of bacterial periplasmic ligand binding proteins (see for example, Sack et al., 1989) and with recent time-resolved ligand binding studies of GluRD S1S2 (Abele et al., 2000). The initial binding of glutamate to domain 1 occurs because this binding site is largely preorganized, even in the apo state. Following this initial contact, shown in Figure 7B, domain closure occurs, and the γ-carboxyl group interacts with the base of helix F and water molecules 1–3 (Figure 7C); we suggest that this step leads to channel activation. In the agonist-bound structures, Lys-730 is proximal to Asp-728. Thus, Lys-730 may act as a switch between the apo and full agonist–bound states; in the apo state it interacts with Glu-705 and in the full agonist state Lys-730 is near Asp-728. Indeed, Asp-728 is located at a hinge region in a transdomain β strand, and the Lys-730 and Asp-728 interaction may stabilize the hinge in the full agonist–bound state.

To connect the conformational changes that we have documented in the ligand binding core to opening of the ion channel gate, we have developed a model of an assembled receptor, shown in Figure 8. This model is based on the following assumptions: (1) AMPA receptors are tetrameric; (2) the transmembrane domain has ~4-fold rotational symmetry; (3) the ligand binding cores are dimeric; and (4) the gate is located proximal to the extracellular surface of the membrane. In our model, agonist binding induces a clockwise screw-axis movement of domain 2 up and away from the channel 4-fold symmetry axis, causing a rotation of the protein near the putative gate. This movement is based on superpositions of the apo and glutamate-bound dimers that show that the two "linker" regions separate by ~5 Å, measured perpendicular to the 2-fold axis, and undergo a rotation of ~5° around the 2-fold axis and a translation of ~4 Å along the 2-fold axis. According to our model, the binding of a partial agonist results in correspondingly smaller conformational changes. Antagonists stabilize the ligand binding core in an open-cleft conformation and thus preclude rotation and separation of the ligand binding regions and subsequent opening of the ion channel gate.

Conclusion

This series of structures marks a novel high-resolution study for a portion of a ligand-gated ion channel in the apo, antagonist-, and agonist-bound states. Comparisons of these five structures have uncovered plausible mechanisms underlying the antagonism, activation, and modulation of iGluRs. Based on the spectrum of conformations presented here, we propose that the substantial degree of domain closure that occurs upon agonist bind-

ing initiates iGluR channel activation. Furthermore, comparison of the full agonist– and partial agonist–bound structures indicates that the channel activation level is dependent upon the conformation of the ligand binding domain and, more specifically, the extent of S1S2 domain closure. In contrast to the large conformational change induced by agonists, the binding of competitive antagonists, such as DNQX, produces minimal domain closure and therefore these ligands do not activate the wild-type receptor. The dimer observed in these crystal forms supports a role for intermolecular interactions in receptor desensitization and suggests that the iGluR tetramer may consist of dimers-of-dimers. Zn^{2+} binding sites and peptide-bond flipping may also be involved in modulation of receptor activity by altering inter- and intrasubunit interactions, respectively. The mechanisms we have put forth to explain the behavior of the AMPA GluR2 receptor may also be germane to the understanding of kainate and NMDA receptors.

Experimental Procedures

Construct Design

The three amino acid changes made to the N terminus of S1S2I, G389R, L390G, and E391A were introduced by way of cassette mutagenesis using the following oligos: PRM1: 5′-CAT GGG CTC AGG AAA TGA CAC TAG TCG CGG TGC AAA CAA AAC TGT GGT G-3′ and PRM2: 5′-GTG ACC ACC ACA GTT TTG TTT GCA CCG CGA CTA GTG TCA TTT CCT GAG CC-3′, where underlined letters indicate mutated bases. The PRM1:PRM2 cassette was cloned into pS1S2I to generate pS1S2I2 using the NcoI and BstEII restriction sites. The sequence at the linker was changed to $MIKK^{506}$-GT-P^{632}IES by strand-overlap extension PCR using the following primers: PRM3: 5′-GAA GGG TAC CCC CAT CGA AAG TGC TGA G-3′, PRM4: 5′-TCG ATG GGG GTA CCC TTC TTG ATC ATG ATA G-3′, PRM5: 5′-GGG CTA CTG TGT TGA CTT-3′, and PRM6: 5′-CTT CTG CGG TAG TCC TC-3′. PRM4 and PRM5 were combined with pS1S2I in one PCR reaction to generate the S1 half of the insert, while PRM3 and PRM6 were used to synthesize the S2 half. In a third PCR reaction, the S1 and S2 PCR products were combined with PRM5 and PRM6 to create the linker insert. The insert was digested with PstI and BglII, cloned into pS1S2I2 that had been digested with the same enzymes, and sequenced.

Activity Assay

Protein production, refolding, and purification were carried out as previously described (Chen et al., 1998). The ^{3}H-AMPA K_d value and DNQX IC_{50} were measured for S1S2J at pH 7.0 and pH 5.0 following previously published protocols (Chen and Gouaux, 1997). The buffer used for the low pH measurements contained 30 mM NaOAc, pH 5.0, instead of 30 mM Tris, pH 7.0. IC_{50} values were also determined for glutamate and kainate at pH 7.0 by competition binding experiments. For competition experiments, 20 nM ^{3}H-AMPA (10.6 Ci/mmol) was used in all samples and either 1 nM–0.1 mM DNQX, 10 pM–500 μM L-glutamate, or 1 nM–1 mM kainate. Ligand binding experiments were carried out in duplicate.

Crystallization

S1S2J was dialyzed extensively against 10 mM HEPES, pH 7.0, 20 mM NaCl, and 1 mM EDTA to remove all traces of glutamate (except for material intended for cocrystallization with glutamate). Final ligand concentrations were: 3 mM DNQX, 10 mM kainate, 2 mM (S)-AMPA, and 10 mM L-glutamate. All crystals were grown at 4°C in hanging drops containing a 1:1 (v/v) ratio of protein solution (7 and 14 mg/ml as determined by OD_{280}) to reservoir solution. DNQX crystallization buffer contained 17%–22% PEG 4000, 0.25–0.4 M ammonium sulfate, and 0.1 M NaOAc at pH 5.0. The apo crystals grew in a condition identical to that for DNQX except that 19%–24% PEG 8000 replaced the PEG 4000 and 10% (v/v) glycerol was included with the protein. Glutamate and AMPA cocrystals grew in 13%–18% PEG 8000, 0.1–0.25 M $Zn(OAc)_2$, and 0.1 M cacodylate at pH 6.5. The kainate crystallization buffer consisted of 8%–15% PEG1450 and 0.1 M NaOAc at pH 5.0. Crystals were soaked in crystallization buffer supplemented with the corresponding ligand and 10%–12% glycerol prior to flash freezing in liquid nitrogen.

Structure Determination

The glutamate- and kainate-S1S2J structures were determined by MR using the S1S2I-kainate structure as the search probe. Taking advantage of its isomorphism with the glutamate crystal form, the AMPA structure was refined by difference Fourier techniques. For all three structures, the refinement protocol began with rigid body refinement followed by a slow-cool simulated-annealing run at 4000 K to reduce model bias. Iterative rounds of model building (including side chains, waters, ligands, and ions) into omit maps and positional and individual B-value refinement were performed until the R_{free} converged. NCS restraints (300 kcal/mol* Å^2) were applied to the three molecules in the glutamate asymmetric unit (a.u.) in the initial rounds of refinement. However, restraints were completely released when the R_{free} reached 0.34. Ligands were modeled into F_o-F_c maps using either the small-molecule crystal structure (Honoré and Lauridsen, 1980; Todeschi et al., 1997) or a rotamer from the O library when the R_{free} dropped below 0.30. Refinement of the kainate structure was stopped when superpositions of the S1S2I- and S1S2J-kainate models revealed no significant differences in the mode of kainate binding and the orientation of the lobes. The rmsd calculated for all Cα atoms between the two kainate structures was 0.61 Å. Because the S1S2I data extended to 1.6 Å and was collected on a crystal grown closer to physiological pH (6.5), we used this structure for the majority of the crystallographic analysis.

The DNQX crystals grew in two different lattices that differed by a doubling of the *c* axis in the larger form. The DNQX structure was determined by a combination of MR and MAD using the larger form prior to discovery of the smaller lattice. A MR solution could only be obtained when the kainate dimer, which was generated by superimposing a S1S2I-kainate complex on each molecule in the glutamate "dimer," was used a search probe. Even though the MR solution had a correlation coefficient of 60.1, extensive refinement only lowered the R_{free} to 40.0%. Maps inspected at this point contained reasonable density for all of domain 1, but the density for most of domain 2 was uninterpretable. Therefore, a 3-wavelength MAD data set was collected on a selenomethionine-derivatized DNQX crystal. Anomalous difference Fourier maps calculated using structure factors obtained from data measured at the selenium K peak and phases from the DNQX molecular replacement structure clearly indicated the location of all 40 selenium sites. SOLVE (Terwilliger and Berendzen, 1999) was used to refine the position and occupancy of the sites and to calculate 4.0 Å MAD phases (figure of merit, FOM, of 0.71). After density modification in DM including solvent flattening, histogram matching, phase extension to 2.5 Å, and 4-fold NCS averaging, the FOM was 0.81. The electron density in these maps was excellent, allowing for an unambiguous repositioning of domain 2. Eventually, a 1.8 Å native data set was collected on the smaller DNQX crystal form, which was solved by molecular replacement (CC = 69.2). A DNQX model constructed from the published x-ray coordinates (Kubicki et al., 1996) was placed into 1.8 Å F_o-F_c density when the R_{free} reached 28.6%. The refined DNQX "dimer" structure was used as the search probe for the apo structure determination (CC = 64.6). IC_{50} measurements at the pH value of the crystallization buffer confirmed that the DNQX affinity is not compromised at pH 5.0.

Apo, kainate, and glutamate data sets were collected using copper Kα radiation and an R-Axis IV area detector. The x-ray beam was focused using a compound reflector geometry to symmetrically image the 300 μm beam (J. Lidestri and W. A. Hendrickson, personal communication). The AMPA data and the DNQX MAD and native data were collected on a Quantum 4 CCD detector at the NSLS beamline X4A. Data for all crystal forms was indexed, scaled, and merged using HKL (Otwinowsky and Minor, 1997). All molecular replacement calculations were performed in AMoRe (Navaza, 1994). Refinements were carried out in X-PLOR (Brünger, 1992). O (Jones and Kjeldgaard, 1997) was used for model building and for displaying maps. Superpositions and various structural analyses were

calculated using LSQMAN (Kleywegt and Jones, 1994) and X-PLOR (Brünger, 1992). The extent of domain "closure" was determined using the script HINGEFIND (Wriggers and Schulten, 1997) implemented in X-PLOR (Brünger, 1992). Using the ApoA structure as a reference state, the rotation required to fit the second domain following superposition of the first is defined as the extent of "domain closure." All other crystallographic calculations were carried out in the CCP4 program suite (*CCP4 Project*, 1994).

Acknowledgments

M. Montoya prepared and characterized the S1S2J construct used in this study. J. Lidestri is thanked for exceptional support and maintenance of the x-ray facility. Y. Liu and J. Williams provided helpful suggestions on structure determination, and Y. Sun and other members of the Gouaux lab assisted with data collection. M. Mayer provided numerous helpful comments. S. Heinemann is acknowledged for providing the GluR2 flop clone. Synchrotron diffraction data was collected at the X4a beamline at the National Synchrotron Light Source and benefited from the helpful advice of C. Ogata. Support for the research was provided by the Klingenstein Foundation, the National Alliance for Research on Schizophrenia and Depression, and the National Institutes of Health.

Received September 8, 2000; revised September 15, 2000.

References

Abele, R., Keinänen, K., and Madden, D.R. (2000). Agonist-induced isomerization in a glutamate receptor ligand-binding domain. A kinetic and mutagenetic analysis. J. Biol. Chem. *275*, 21355–21363.

Abele, R., Svergun, D., Keinänen, K., Koch, M.H., and Madden, D.R. (1999). A molecular envelope of the ligand-binding domain of a glutamate receptor in the presence and absence of agonist. Biochemistry *38*, 10949–10957.

Andersen, P.H., Tygesen, C.K., Rasmussen, J.S., Soegaard-Nielsen, L., Hansen, A., Hansen, K., Kiemer, A., and Stidsen, C.E. (1996). Stable expression of homomeric AMPA-selective glutamate receptors in BHK cells. Eur. J. Pharmacol. *311*, 95–100.

Armstrong, N., Sun, Y., Chen, G.-Q., and Gouaux, E. (1998). Structure of a glutamate receptor ligand binding core in complex with kainate. Nature *395*, 913–917.

Assaf, S.Y., and Chung, S.H. (1984). Release of endogenous Zn2+ from brain tissue during activity. Nature *308*, 734–736.

Borges, K., and Dingledine, R. (1998). AMPA receptors: molecular and functional diversity. Prog. Brain Res. *116*, 153–170.

Boulter, J., Hollmann, M., O'Shea-Greenfield, A., Hartley, M., Deneris, E., Maron, C., and Heinemann, S. (1990). Molecular cloning and functional expression of glutamate receptor subunit genes. Science *249*, 1033–1037.

Bräuner-Osborne, H., Egebjerg, J., Nielsen, E.O., Madsen, U., and Krogsgaard-Larsen, P. (2000). Ligands for glutamate receptors: design and therapeutic propects. J. Med. Chem. *43*, 2609–2645.

Brünger, A.T. (1992). X-PLOR. Version 3.1. A System for X-Ray Crystallography and NMR (New Haven, CT: Yale University Press).

CCP4 Project, N. (1994). The *CCP4* suite: programs for protein crystallography. Acta Crystallogr. *D50*, 760–763.

Chen, G.Q., and Gouaux, E. (1997). Overexpression of a glutamate receptor (GluR2) ligand binding domain in *Escherichia coli*: application of a novel protein folding screen. Proc. Natl. Acad. Sci. USA *94*, 13431–13436.

Chen, G.Q., Sun, Y., Jin, R., and Gouaux, E. (1998). Probing the ligand binding domain of the GluR2 receptor by proteolysis and deletion mutagenesis defines domain boundaries and yields a crystallizable construct. Protein Sci. *7*, 2623–2630.

Chen, G.Q., Cui, C., Mayer, M.L., and Gouaux, E. (1999). Functional characterization of a potassium-selective prokaryotic glutamate receptor. Nature *402*, 817–821.

Chittajallu, R., Braithwaite, S.P., Clarke, V.R., and Henley, J.M. (1999). Kainate receptors: subunits, synaptic localization and function. Trends Pharmacol. Sci. *20*, 26–35.

Conte, L.L., Chothia, C., and Janin, J. (1999). The atomic structure of protein-protein recognition sites. J. Mol. Biol. *285*, 2177–2198.

Dingledine, R., Borges, K., Bowie, D., and Traynelis, S.F. (1999). The glutamate receptor ion channels. Pharmacol. Rev. *51*, 7–61.

Doyle, D.A., Morais Cabral, J., Pfuetzner, R.A., Kuo, A., Gulbis, J.M., Cohen, S.L., Chait, B.T., and MacKinnon, R. (1998). The structure of the potassium channel: molecular basis of K+ conduction and selectivity. Science *280*, 69–77.

Dreixler, J.C., and Leonard, J.P. (1994). Subunit-specific enhancement of glutamate receptor responses by zinc. Brain Res. Mol. Brain Res. *22*, 144–150.

Emsley, J., Knight, C.G., Farndale, R.W., Barnes, M.J., and Liddington, R.C. (2000). Structural basis of collagen recognition by integrin $\alpha 2\beta 1$. Cell *101*, 47–56.

Flocco, M.M., and Mowbray, S.L. (1994). The 1.9 Å x-ray structure of a closed unliganded form of the periplasmic glucose/galactose receptor from *Salmonella typhimurium*. J. Biol. Chem. *269*, 8931–8936.

Hendrickson, W.A. (1991). Determination of macromolecular structures from anomalous diffraction of synchrotron radiation. Science *254*, 51–58.

Hendrickson, W.A., Horton, J.R., and LeMaster, D.M. (1990). Selenomethionyl proteins produced for analysis by multiwavelength anomalous diffraction (MAD): a vehicle for direct determination of three-dimensional structure. EMBO J. *9*, 1665–1672.

Hennegriff, M., Arai, A., Kessler, M., Vanderklish, P., Mutneja, M.S., Rogers, G., Neve, R.L., and Lynch, G. (1997). Stable expression of recombinant AMPA receptor subunits: binding affinities and effects of allosteric modulators. J. Neurochem. *68*, 2424–2434.

Hollmann, M., and Heinemann, S. (1994). Cloned glutamate receptors. Annu. Rev. Neurosci. *17*, 31–108.

Honoré, T., and Lauridsen, J. (1980). Structural analogues of ibotenic acid. Syntheses of 4-methyl-homoibotenic acid and AMPA, including the crystal structure of AMPA monohydrate. Acta Chemica Scandinavica B *34*, 235–240.

Honoré, T., Davies, S.N., Drejer, J., Fletcher, E.J., Jacobsen, P., Lodge, D., and Nielsen, F.E. (1988). Quinoxalinediones: potent competitive non-NMDA glutamate receptor antagonists. Science *241*, 701–703.

Hsiao, C.-D., Sun, Y.-J., Rose, J., and Wang, B.-C. (1996). The crystal structure of glutamine-binding protein from *Escherichia coli*. J. Mol. Biol. *262*, 225–242.

Ivanovic, A., Reiländer, H., Laube, B., and Kuhse, J. (1998). Expression and initial characterization of a soluble glycine binding domain of the N-methyl-D-aspartate receptor NR1 subunit. J. Biol. Chem. *273*, 19933–19937.

Jones, T.A., and Kjeldgaard, M. (1997). Electron-density map interpretation. Methods Enzymol. *277*, 173–208.

Kashiwabuchi, N., Ikeda, K., Araki, K., Hirano, T., Shibuki, K., Takayama, C., Inoue, Y., Kutsuwada, T., Yagi, T., and Kang, Y. (1995). Impairment of motor coordination, Purkinje cell synapse formation, and cerebellar long-term depression in GluR $\delta 2$ mutant mice. Cell *81*, 245–252.

Kawamoto, S., Uchino, S., Xin, K.Q., Hattori, S., Hamajima, K., Fukushima, J., Mishina, M., and Okuda, K. (1997). Arginine-481 mutation abolishes ligand-binding of the AMPA-selective glutamate receptor channel $\alpha 1$-subunit. Brain Res. Mol. Brain Res. *47*, 339–344.

Keinänen, K., Jouppila, A., and Kuusinen, A. (1998). Characterization of the kainate-binding domain of the glutamate receptor GluR-6 subunit. Biochem. J. *330*, 1461–1467.

Keinänen, K., Wisden, W., Sommer, B., Werner, P., Herb, A., Verdoorn, T.A., Sakmann, B., and Seeburg, P.H. (1990). A family of AMPA-selective glutamate receptors. Science *249*, 556–560.

Kessler, M., Arai, A., Quan, A., and Lynch, G. (1996). Effect of cyclothiazide on binding properties of AMPA-type glutamate receptors: lack of competition between cyclothiazide and GYKI 52466. Mol. Pharmacol. *49*, 123–131.

Kiskin, N.I., Krishtal, O.A., and Tsyndrenko, A.Ya. (1986). Excitatory amino acid receptors in hippocampal neurons: kainate fails to desensitize them. Neurosci. Lett. *63*, 225–230.

Kleywegt, G.J., and Jones, T.A. (1994). A super position. In CCP4/ESF-EACBM Newsletter on Protein Crystallography, pp. 9–14.

Kohda, K., Wang, Y., and Yuzaki, M. (2000). Mutation of a glutamate receptor motif reveals its role in gating and δ2 receptor channel properties. Nat. Neurosci. *3*, 315–322.

Koike, M., Tsukada, S., Tsuzuki, K., Kijima, H., and Ozawa, S. (2000). Regulation of kinetic properties of GluR2 AMPA receptor channels by alternative splicing. J. Neurosci. *20*, 2166–2174.

Kubicki, M., Kindopp, T.W., Capparelli, M.V., and Codding, P.W. (1996). Hydrogen-bonding patterns in 1,4-dihydro-2,3-quinoxalinediones: ligands for the glycine modulatory site on the NMDA receptor. Acta Crystallogr. B *52*, 487–499.

Kuusinen, A., Arvola, M., and Keinänen, K. (1995). Molecular dissection of the agonist binding site of an AMPA receptor. EMBO J. *14*, 6327–6332.

Kuusinen, A., Abele, R., Madden, D.R., and Keinänen, K. (1999). Oligomerization and ligand-binding properties of the ectodomain of the α-amino-3-hydroxy-5-methyl-4-isoxazole propionic acid receptor subunit GluRD. J. Biol. Chem. *274*, 28937–28943.

Lampinen, M., Pentikäinen, O., Johnson, M.S., and Keinänen, K. (1998). AMPA receptors and bacterial periplasmic amino acid-binding proteins share the ionic mechanism of ligand recognition. EMBO J. *17*, 4704–4711.

Laube, B., Hirai, H., Sturgess, M., Betz, H., and Kuhse, J. (1997). Molecular determinants of agonist discrimination by NMDA receptor subunits: analysis of the glutamate binding site on the NR2B subunit. Neuron *18*, 493–503.

Lerma, J., Morales, M., Vicente, M.A., and Herreras, O. (1997). Glutamate receptors of the kainate type and synaptic transmission. Trends Neurosci. *20*, 9–12.

Leuschner, W.D., and Hoch, W. (1999). Subtype-specific assembly of α-amino-3-hydroxy-5-methyl-4-isoxazole propionic acid receptor subunits is mediated by their N-terminal domains. J. Biol. Chem. *274*, 16907–16916.

Lomeli, H., Sprengel, R., Laurie, D.J., Kohr, G., Herb, A., Seeburg, P.H., and Wisden, W. (1993). The rat δ1 and δ2 subunits extend the excitatory amino acid receptor family. FEBS Lett. *315*, 318–322.

Lomeli, H., Mosbacher, J., Melcher, T., Hoger, T., Geiger, J.R.P., Kuner, T., Monyer, H., Higuchi, M., Bach, A., and Seeburg, P.H. (1994). Control of kinetic properties of AMPA receptors channels by nuclear RNA editing. Science *266*, 1709–1713.

Mano, I., Lamed, Y., and Teichberg, V.I. (1996). A Venus flytrap mechanism for activation and desensitization of α-amino-3-hydroxy-5-methyl-4-isoxazole propionic acid receptors. J. Biol. Chem. *271*, 15299–15302.

Matzen, L., Engesgaard, A., Ebert, B., Didriksen, M., Frolund, B., Krogsgaard-Larsen, P., and Jaroszewski, J.W. (1997). AMPA receptor agonists: synthesis, protolytic properties, and pharmacology of 3-isothiazolol bioisosteres of glutamic acid. J. Med. Chem. *40*, 520–527.

Mayer, M.L., and Vyklicky, L., Jr. (1989). The action of zinc on synaptic transmission and neuronal excitability in cultures of mouse hippocampus. J. Physiol. Lond. *415*, 351–365.

Moller, E.H., Egebjerg, J., Brehm, L., Stensbol, T.B., Johansen, T.N., Madsen, U., and Krogsgaard-Larsen, P. (1999). Resolution, absolute stereochemistry, and enantiopharmacology of the GluR1-4 and GluR5 antagonist 2-amino-3-[5-tert-butyl-3-(phosphonomethoxy)-4-isoxazolyl]propionic acid. Chirality *11*, 752–759.

Mosbacher, J., Schoepfer, R., Monyer, H., Burnashev, N., Seeburg, P.H., and Ruppersberg, J.P. (1994). A molecular determinant for submillisecond desensitization in glutamate receptors. Science *266*, 1059–1062.

Nakanishi, S., and Masu, M. (1994). Molecular diversity and functions of glutamate receptors. Annu. Rev. Biophys. Biomol. Struct. *23*, 319–348.

Nakanishi, N., Shneider, N.A., and Axel, R. (1990). A family of glutamate receptor genes: evidence for the formation of heteromultimeric receptors with distinct channel properties. Neuron *5*, 569–581.

Nar, H., Messerschmidt, A., Huber, R., van de Kamp, M., and Canters, G.W. (1991). Crystal structure analysis of oxidized *Pseudomonas aeruginosa* azurin at pH 5.5 and pH 9.0. A pH-induced conformational transition involves a peptide bond flip. J. Mol. Biol. *221*, 765–772.

Navaza, J. (1994). *AMoRe*: An automated package for molecular replacement. Acta Crystallogr. A *50*, 157–163.

North, R.A., and Barnard, E.A. (1997). Nucleotide receptors. Curr. Opin. Neurobiol. *7*, 346–357.

O'Hara, P.J., Sheppard, P.O., Thogersen, H., Venezia, D., Haldeman, B.A., McGrane, V., Houamed, K.M., Thomsen, C., Gilbert, T.L., and Mulvihill, E.R. (1993). The ligand-binding domain in metabotropic glutamate receptors is related to bacterial periplasmic binding proteins. Neuron *11*, 41–52.

Okamoto, T., Sekiyama, N., Otsu, M., Shimada, Y., Sato, A., Nakanishi, S., and Jingami, H. (1998). Expression and purification of the extracellular ligand binding region of metabotropic glutamate receptor subtype 1. J. Biol. Chem. *273*, 13089–13096.

Olah, G.A., Trakhanov, S., Trewhella, J., and Quiocho, F.A. (1993). Leucine/isoleucine/valine-binding protein contracts upon binding of ligand. J. Biol. Chem. *268*, 16241–16247.

Otwinowsky, Z., and Minor, W. (1997). Processing of x-ray diffraction data collected in oscillation mode. Methods Enzymol. *276*, 307–326.

Paas, Y. (1998). The macro- and microarchitectures of the ligand-binding domain of glutamate receptors. Trends Neurosci. *21*, 117–125.

Partin, K.M., Patneau, D.K., and Mayer, M.L. (1994). Cyclothiazide differentially modulates desensitization of α-amino-3-hydroxy-5-methyl-4-isoxazole propionic acid receptor splice variants. Mol. Pharmacol. *46*, 129–138.

Partin, K.M., Bowie, D., and Mayer, M.L. (1995). Structural determinants of allosteric regulation in alternatively spliced AMPA receptors. Neuron *14*, 833–843.

Partin, K.M., Fleck, M.W., and Mayer, M.L. (1996). AMPA receptor flip/flop mutants affecting deactivation, desensitization, and modulation by cyclothiazide, aniracetam, and thiocyanate. J. Neurosci. *16*, 6634–6647.

Patneau, D.K., Vyklicky, L., and Mayer, M.L. (1993). Hippocampal neurons exhibit cyclothiazide-sensitive rapidly desensitizing responses to kainate. J. Neurosci. *13*, 3496–3509.

Perez-Clausell, J., and Danscher, G. (1985). Intravesicular localization of zinc in rat telencephalic boutons. A histochemical study. Brain Res. *337*, 91–98.

Perozo, E., Cortes, D.M., and Cuello, L.G. (1999). Structural rearrangements underlying K+-channel activation gating. Science *285*, 73–78.

Romano, C., Yang, W.L., and O'Malley, K.L. (1996). Metabotropic glutamate receptor 5 is a disulfide-linked dimer. J. Biol. Chem. *271*, 28612–28616.

Romero, A., Caldeira, J., Legall, J., Moura, I., Moura, J.J., and Romao, M.J. (1996). Crystal structure of flavodoxin from *Desulfovibrio desulfuricans* ATCC 27774 in two oxidation states. Eur. J. Biochem. *239*, 190–196.

Sack, J.S., Trakhanov, S.D., Tsigannik, I.H., and Quiocho, F.A. (1989). Structure of the L-leucine-binding protein refined at 2.4 Å resolution and comparison with the Leu/Ile/Val-binding protein structure. J. Mol. Biol. *206*, 193–207.

Seeburg, P.H. (1993). The TINS/TiPS Lecture. The molecular biology of mammalian glutamate receptor channels. Trends Neurosci. *16*, 359–365.

Smith, C.T., Wang, L.Y., and Howe, J.R. (2000). Heterogeneous conductance levels of native AMPA receptors. J. Neurosci. *20*, 2073–2085.

Sommer, B., Keinänen, K., Verdoorn, T.A., Wisden, W., Burnashev, N., Herb, A., Kohler, M., Takagi, T., Sakmann, B., and Seeburg, P.H. (1990). Flip and flop: a cell-specific functional switch in glutamate-operated channels of the CNS. Science *249*, 1580–1585.

Stern-Bach, Y., Bettler, B., Hartley, M., Sheppard, P.O., O'Hara, P.J., and Heinemann, S.F. (1994). Agonist selectivity of glutamate receptors is specified by two domains structurally related to bacterial amino acid-binding proteins. Neuron *13*, 1345–1357.

Stern-Bach, Y., Russo, S., Neuman, M., and Rosenmund, C. (1998). A point mutation in the glutamate binding site blocks desensitization of AMPA receptors. Neuron *21*, 907–918.

Sun, Y.-J., Rose, J., Wang, B.-C., and Hsiao, C.-D. (1998). The structure of glutamine-binding protein complexed with glutamine at 1.94 Å resolution: comparisons with other amino acid binding proteins. J. Mol. Biol. *278*, 219–229.

Swanson, G.T., Gereau, R.W., Green, T., and Heinemann, S.F. (1997a). Identification of amino acid residues that control functional behavior in GluR5 and GluR6 kainate receptors. Neuron *19*, 913–926.

Swanson, G.T., Kamboj, S.K., and Cull-Candy, S.G. (1997b). Single-channel properties of recombinant AMPA receptors depend on RNA editing, splice variation, and subunit composition. J. Neurosci. *17*, 58–69.

Taverna, F., Xiong, Z., Brandes, L., Roder, J.C., Salter, M.W., and MacDonald, J.F. (2000). The lurcher mutation of an α-amino-3-hydroxy-5-methyl-4-isoxazolepropionic acid receptor subunit enhances potency of glutamate and converts an antagonist to an agonist. J. Biol. Chem. *275*, 8475–8479.

Terwilliger, T.C., and Berendzen, J. (1999). Automated MAD and MIR structure solution. Acta Crystallogr. D *55*, 849–861.

Todeschi, N., Gharbi-Benarous, J., and Girault, J.-P. (1997). Structure of kainic acid totally elucidated by NMR and molecular modeling. Bioorg. Med. Chem. *5*, 1943–1957.

Trussell, L.O., Thio, L.L., Zorumski, C.F., and Fischbach, G.D. (1988). Rapid desensitization of glutamate receptors in vertebrate central neurons. Proc. Natl. Acad. Sci. USA *85*, 4562–4566.

Unwin, N. (1998). The nicotinic acetylcholine receptor of the Torpedo electric ray. J. Struct. Biol. *121*, 181–190.

Wallace, A.C., Laskowski, R.A., and Thornton, J.M. (1995). LIGPLOT: a program to generate schematic diagrams of protein-ligand interactions. Prot. Eng. *8*, 127–134.

Wheal, H., and Thomson, A. (1995). Excitory Amino Acids and Synaptic Transmission, Second Edition (San Diego, CA: Academic Press Inc.).

Wo, Z.G., and Oswald, R.E. (1995). Unraveling the modular design of glutamate-gated ion channels. Trends Neurosci. *18*, 161–168.

Wolf, A., Shaw, E.W., Nikaido, K., and Ames, G.F. (1994). The histidine-binding protein undergoes conformational changes in the absence of ligand as analyzed with conformation-specific monoclonal antibodies. J. Biol. Chem. *269*, 23051–23058.

Wriggers, W., and Schulten, K. (1997). Protein domain movements: detection of rigid domains and visualization of hinges in comparisons of atomic coordinates. Proteins *29*, 1–14.

Yamakura, T., and Shimoji, K. (1999). Subunit- and site-specific pharmacology of the NMDA receptor channel. Prog. Neurobiol. *59*, 279–298.

Zagotta, W.N., and Siegelbaum, S.A. (1996). Structure and function of cyclic nucleotide-gated channels. Annu. Rev. Neurosci. *19*, 235–263.

Zuo, J., De Jager, P.L., Takahashi, K.A., Jiang, W., Linden, D.J., and Heintz, N. (1997). Neurodegeneration in Lurcher mice caused by mutation in δ2 glutamate receptor gene. Nature *388*, 769–773.

Protein Data Bank ID Codes

Coordinates for the S1S2J-glutamate, -DNQX, -AMPA, -apo, and -kainate structures and the 1.6 Å S1S2I-kainate structure have been deposited in the Protein Data Bank under ID codes 1FTJ, 1FTL, 1FTM, 1FTO, 1FW0, and 1FTK, respectively.